arXiv:hep-ex/0106051v1 13 Jun 2001

EUROPEAN ORGANIZATION FOR NUCLEAR RESEARCH (CERN)

CERN-EP/2001-039
May 21st, 2001

Study of the fragmentation of b quarks into B mesons at the Z peak

The ALEPH Collaboration*)

Abstract

The fragmentation of b quarks into B mesons is studied with four million hadronic Z decays collected by the ALEPH experiment during the years 1991–1995. A semi-exclusive reconstruction of $B \to \ell\nu D^{(\star)}$ decays is performed, by combining lepton candidates with fully reconstructed $D^{(\star)}$ mesons while the neutrino energy is estimated from the missing energy of the event.

The mean value of x_B^{wd}, the energy of the weakly-decaying B meson normalised to the beam energy, is found to be

$$\langle x_B^{\mathrm{wd}} \rangle = 0.716 \ \pm 0.006\,(\mathrm{stat}) \ \pm 0.006\,(\mathrm{syst})$$

using a model-independent method; the corresponding value for the energy of the leading B meson is $\langle x_B^{\mathrm{L}} \rangle = 0.736 \ \pm 0.006\,(\mathrm{stat}) \ \pm 0.006\,(\mathrm{syst})$. The reconstructed spectra are compared with different fragmentation models.

To be submitted to Physics Letters

---

*) See next pages for the list of authors

The ALEPH Collaboration

A. Heister, S. Schael

Physikalisches Institut das RWTH-Aachen, D-52056 Aachen, Germany

R. Barate, I. De Bonis, D. Decamp, C. Goy, J.-P. Lees, E. Merle, M.-N. Minard, B. Pietrzyk

Laboratoire de Physique des Particules (LAPP), IN^{2}P^3-CNRS, F-74019 Annecy-le-Vieux Cedex, France

S. Bravo, M.P. Casado, M. Chmeissani, J.M. Crespo, E. Fernandez, M. Fernandez-Bosman, Ll. Garrido,[15] E. Graugés, M. Martinez, G. Merino, R. Miquel,[27] Ll.M. Mir,[27] A. Pacheco, H. Ruiz

Institut de Física d'Altes Energies, Universitat Autònoma de Barcelona, E-08193 Bellaterra (Barcelona), Spain[7]

A. Colaleo, D. Creanza, M. de Palma, G. Iaselli, G. Maggi, M. Maggi, S. Nuzzo, A. Ranieri, G. Raso,[23] F. Ruggieri, G. Selvaggi, L. Silvestris, P. Tempesta, A. Tricomi,[3] G. Zito

Dipartimento di Fisica, INFN Sezione di Bari, I-70126 Bari, Italy

X. Huang, J. Lin, Q. Ouyang, T. Wang, Y. Xie, R. Xu, S. Xue, J. Zhang, L. Zhang, W. Zhao

Institute of High Energy Physics, Academia Sinica, Beijing, The People's Republic of China[8]

D. Abbaneo, P. Azzurri, G. Boix,[6] O. Buchmüller, M. Cattaneo, F. Cerutti, B. Clerbaux, G. Dissertori, H. Drevermann, R.W. Forty, M. Frank, T.C. Greening, J.B. Hansen, J. Harvey, P. Janot, B. Jost, M. Kado, P. Mato, A. Moutoussi, F. Ranjard, L. Rolandi, D. Schlatter, O. Schneider,[2] P. Spagnolo, W. Tejessy, F. Teubert, E. Tournefier,[25] J. Ward

European Laboratory for Particle Physics (CERN), CH-1211 Geneva 23, Switzerland

Z. Ajaltouni, F. Badaud, A. Falvard,[22] P. Gay, P. Henrard, J. Jousset, B. Michel, S. Monteil, J-C. Montret, D. Pallin, P. Perret, F. Podlyski

Laboratoire de Physique Corpusculaire, Université Blaise Pascal, IN^{2}P^3-CNRS, Clermont-Ferrand, F-63177 Aubière, France

J.D. Hansen, J.R. Hansen, P.H. Hansen, B.S. Nilsson, A. Wäänänen

Niels Bohr Institute, DK-2100 Copenhagen, Denmark[9]

A. Kyriakis, C. Markou, E. Simopoulou, A. Vayaki, K. Zachariadou

Nuclear Research Center Demokritos (NRCD), GR-15310 Attiki, Greece

A. Blondel,[12] G. Bonneaud, J.-C. Brient, A. Rougé, M. Rumpf, M. Swynghedauw, M. Verderi, H. Videau

Laboratoire de Physique Nucléaire et des Hautes Energies, Ecole Polytechnique, IN^{2}P^3-CNRS, F-91128 Palaiseau Cedex, France

V. Ciulli, E. Focardi, G. Parrini

Dipartimento di Fisica, Università di Firenze, INFN Sezione di Firenze, I-50125 Firenze, Italy

A. Antonelli, M. Antonelli, G. Bencivenni, G. Bologna,[4] F. Bossi, P. Campana, G. Capon, V. Chiarella, P. Laurelli, G. Mannocchi,[5] F. Murtas, G.P. Murtas, L. Passalacqua, M. Pepe-Altarelli[24]

Laboratori Nazionali dell'INFN (LNF-INFN), I-00044 Frascati, Italy

A.W. Halley, J.G. Lynch, P. Negus, V. O'Shea, C. Raine, A.S. Thompson

Department of Physics and Astronomy, University of Glasgow, Glasgow G12 8QQ,United Kingdom[10]

S. Wasserbaech

Department of Physics, Haverford College, Haverford, PA 19041-1392, U.S.A.

R. Cavanaugh, S. Dhamotharan, C. Geweniger, P. Hanke, G. Hansper, V. Hepp, E.E. Kluge, A. Putzer, J. Sommer, K. Tittel, S. Werner,[19] M. Wunsch[19]

Kirchhoff-Institut für Physik, Universität Heidelberg, D-69120 Heidelberg, Germany[16]

R. Beuselinck, D.M. Binnie, W. Cameron, P.J. Dornan, M. Girone,[1] N. Marinelli, J.K. Sedgbeer, J.C. Thompson[14]

Department of Physics, Imperial College, London SW7 2BZ, United Kingdom[10]

V.M. Ghete, P. Girtler, E. Kneringer, D. Kuhn, G. Rudolph

Institut für Experimentalphysik, Universität Innsbruck, A-6020 Innsbruck, Austria[18]

E. Bouhova-Thacker, C.K. Bowdery, A.J. Finch, F. Foster, G. Hughes, R.W.L. Jones,[1] M.R. Pearson, N.A. Robertson

Department of Physics, University of Lancaster, Lancaster LA1 4YB, United Kingdom[10]

I. Giehl, K. Jakobs, K. Kleinknecht, G. Quast, B. Renk, E. Rohne, H.-G. Sander, H. Wachsmuth, C. Zeitnitz

Institut für Physik, Universität Mainz, D-55099 Mainz, Germany[16]

A. Bonissent, J. Carr, P. Coyle, O. Leroy, P. Payre, D. Rousseau, M. Talby

Centre de Physique des Particules, Université de la Méditerranée, IN^{2}P^3-CNRS, F-13288 Marseille, France

M. Aleppo, F. Ragusa

Dipartimento di Fisica, Università di Milano e INFN Sezione di Milano, I-20133 Milano, Italy

A. David, H. Dietl, G. Ganis,[26] K. Hüttmann, G. Lütjens, C. Mannert, W. Männer, H.-G. Moser, R. Settles, H. Stenzel, W. Wiedenmann, G. Wolf

Max-Planck-Institut für Physik, Werner-Heisenberg-Institut, D-80805 München, Germany[16]

J. Boucrot,[1] O. Callot, M. Davier, L. Duflot, J.-F. Grivaz, Ph. Heusse, A. Jacholkowska,[22] J. Lefrançois, J.-J. Veillet, I. Videau, C. Yuan

Laboratoire de l'Accélérateur Linéaire, Université de Paris-Sud, IN^{2}P^3-CNRS, F-91898 Orsay Cedex, France

G. Bagliesi, T. Boccali, G. Calderini, L. Foà, A. Giammanco, A. Giassi, F. Ligabue, A. Messineo, F. Palla, G. Sanguinetti, A. Sciabà, G. Sguazzoni, R. Tenchini,[1] A. Venturi, P.G. Verdini

Dipartimento di Fisica dell'Università, INFN Sezione di Pisa, e Scuola Normale Superiore, I-56010 Pisa, Italy

G.A. Blair, G. Cowan, M.G. Green, T. Medcalf, A. Misiejuk, J.A. Strong, P. Teixeira-Dias, J.H. von Wimmersperg-Toeller

Department of Physics, Royal Holloway & Bedford New College, University of London, Egham, Surrey TW20 OEX, United Kingdom[10]

R.W. Clifft, T.R. Edgecock, P.R. Norton, I.R. Tomalin

Particle Physics Dept., Rutherford Appleton Laboratory, Chilton, Didcot, Oxon OX11 OQX, United Kingdom[10]

B. Bloch-Devaux,[1] P. Colas, S. Emery, W. Kozanecki, E. Lançon, M.-C. Lemaire, E. Locci, P. Perez, J. Rander, J.-F. Renardy, A. Roussarie, J.-P. Schuller, J. Schwindling, A. Trabelsi,[21] B. Vallage

CEA, DAPNIA/Service de Physique des Particules, CE-Saclay, F-91191 Gif-sur-Yvette Cedex, France[17]

N. Konstantinidis, A.M. Litke, G. Taylor

Institute for Particle Physics, University of California at Santa Cruz, Santa Cruz, CA 95064, USA[13]

C.N. Booth, S. Cartwright, F. Combley, M. Lehto, L.F. Thompson

Department of Physics, University of Sheffield, Sheffield S3 7RH, United Kingdom[10]

K. Affholderbach, A. Böhrer, S. Brandt, C. Grupen, A. Ngac, G. Prange, U. Sieler

Fachbereich Physik, Universität Siegen, D-57068 Siegen, Germany[16]

G. Giannini

Dipartimento di Fisica, Università di Trieste e INFN Sezione di Trieste, I-34127 Trieste, Italy

J. Rothberg

Experimental Elementary Particle Physics, University of Washington, Seattle, WA 98195 U.S.A.

S.R. Armstrong, K. Cranmer, P. Elmer, D.P.S. Ferguson, Y. Gao,[20] S. González, O.J. Hayes, H. Hu, S. Jin, J. Kile, P.A. McNamara III, J. Nielsen, W. Orejudos, Y.B. Pan, Y. Saadi, I.J. Scott, J. Walsh, Sau Lan Wu, X. Wu, G. Zobernig

Department of Physics, University of Wisconsin, Madison, WI 53706, USA[11]

---

[1] Also at CERN, 1211 Geneva 23, Switzerland.

[2] Now at Université de Lausanne, 1015 Lausanne, Switzerland.

[3] Also at Dipartimento di Fisica di Catania and INFN Sezione di Catania, 95129 Catania, Italy.

[4] Deceased.

[5] Also Istituto di Cosmo-Geofisica del C.N.R., Torino, Italy.

[6] Supported by the Commission of the European Communities, contract ERBFMBICT982894.

[7] Supported by CICYT, Spain.

[8] Supported by the National Science Foundation of China.

[9] Supported by the Danish Natural Science Research Council.

[10] Supported by the UK Particle Physics and Astronomy Research Council.

[11] Supported by the US Department of Energy, grant DE-FG0295-ER40896.

[12] Now at Departement de Physique Corpusculaire, Université de Genève, 1211 Genève 4, Switzerland.

[13] Supported by the US Department of Energy, grant DE-FG03-92ER40689.

[14] Also at Rutherford Appleton Laboratory, Chilton, Didcot, UK.

[15] Permanent address: Universitat de Barcelona, 08208 Barcelona, Spain.

[16] Supported by the Bundesministerium für Bildung, Wissenschaft, Forschung und Technologie, Germany.

[17] Supported by the Direction des Sciences de la Matière, C.E.A.

[18] Supported by the Austrian Ministry for Science and Transport.

[19] Now at SAP AG, 69185 Walldorf, Germany.

[20] Also at Department of Physics, Tsinghua University, Beijing, The People's Republic of China.

[21] Now at Département de Physique, Faculté des Sciences de Tunis, 1060 Le Belvédère, Tunisia.

[22] Now at Groupe d' Astroparticules de Montpellier, Université de Montpellier II, 34095 Montpellier, France.

[23] Also at Dipartimento di Fisica e Tecnologie Relative, Università di Palermo, Palermo, Italy.

[24] Now at CERN, 1211 Geneva 23, Switzerland.

[25] Now at ISN, Institut des Sciences Nucléaires, 53 Av. des Martyrs, 38026 Grenoble, France.

[26] Now at INFN Sezione di Roma II, Dipartimento di Fisica, Universitá di Roma Tor Vergata, 00133 Roma, Italy.

[27] Now at LBNL, Berkeley, CA 94720, U.S.A.

1 Introduction

The process of hadron production at e^+e^- colliders is usually modelled as the convolution of a perturbative part (hard gluon radiation for energies above approximately 1 GeV) and a non-perturbative part, called hadronisation or fragmentation, in which the quarks are confined in colourless hadrons. While the first step is in principle calculable, the fragmentation needs a phenomenological approach and is usually parametrised in terms of the variable

$$z \equiv \frac{\left(E + p_{\parallel}\right)_{\mathrm{hadron}}}{(E+p)_{\mathrm{quark}}} \quad , \tag{1}$$

where $p_{\parallel}$ is the hadron's momentum along the direction of the quark, and $(E+p)_{\mathrm{quark}}$ is the sum of the quark energy and momentum just before fragmentation, i.e. taking into account initial and final state photon radiation, and hard gluon emission.

With this definition, the fragmentation process can be described in terms of the probability of a hadron H to be generated with a given z, called $D_q^H(z)$, where q is the flavour of the generating quark. In this paper the fragmentation of b quarks is studied.

The fraction z is not accessible experimentally, and hence a direct reconstruction of $D_b^H(z)$ is not possible. The energy spectrum of b hadrons is therefore described in terms of the scaled energy x_b, defined as the ratio of the heavy hadron energy to the beam energy

$$x_b \equiv \frac{E_{\mathrm{had}}}{E_{\mathrm{beam}}} \quad . \tag{2}$$

In contrast to the z variable, the effects of initial and final state radiation and hard gluon emission are not unfolded.

In the analysis presented, the energy of B mesons is reconstructed using a partially exclusive method: semileptonic decays $B \to \ell\nu D^{(\star)}$ are identified by pairing lepton candidates with fully reconstructed $D^{(\star)}$ mesons; the scaled energy of the weakly-decaying B meson is then computed adding an estimate of the neutrino energy. Five channels are chosen because of their good signal purity and statistical significance; they are shown in Table 1.

In the following x_B^{obs} indicates the reconstructed energy of B meson candidates, x_B^{wd} the energy of weakly decaying B mesons, corrected for detector acceptance and resolution; x_B^{L} stands for the corrected scaled energy of the leading B meson, that is the first meson produced in the fragmentation process, which can also be a heavier resonance ($B^\star$, $B^{\star\star}$).

Channel	Decay chain		
1	$B^0 \to \ell\nu D^\star$	$D^\star \to D^0\pi_{\mathrm{s}}$	$D^0 \to K\pi$
2	$B^0 \to \ell\nu D^\star$	$D^\star \to D^0\pi_{\mathrm{s}}$	$D^0 \to K\pi\pi\pi$
3	$B \to \ell\nu D^0$		$D^0 \to K\pi$
4	$B^0 \to \ell\nu D$		$D \to K\pi\pi$
5	$B^0 \to \ell\nu D^\star$	$D^\star \to D^0\pi_{\mathrm{s}}$	$D^0 \to K\pi\pi^0$

Table 1: B-decay channels used in the analysis.

The analysis uses the full LEP I statistics collected by ALEPH between 1991 and 1995, amounting to almost four million hadronic Z decays. Recently this data set has been reprocessed using improved reconstruction algorithms. The main benefits for this analysis are related to the enhanced secondary vertex reconstruction efficiency and the improved particle identification. A discussion of the reprocessing can be found in [1].

After a description of the ALEPH detector, the selection of $B \to \ell\nu D^{(\star)}$ decays is detailed in Section 3. In Section 4 the reconstruction of the B meson energy is described, followed by the extraction of the spectrum and comparison with the predictions of different models in Section 5. Systematic errors are discussed in Section 6, and checks on the self-consistency and robustness of the analysis are presented in Section 7.

2 The ALEPH detector

The ALEPH detector and its performance are described in detail elsewhere [2, 3]. A high resolution vertex detector (VDET) consisting of two layers of silicon with double-sided readout measures $r\phi$ and z coordinates at average radii of 6.5 cm and 11.3 cm, with 12 μm resolution at normal incidence. The VDET provides full azimuthal coverage, and polar angle coverage to $|\cos\theta| < 0.85$ for the inner layer and $|\cos\theta| < 0.69$ for both layers. Outside VDET, particles traverse the inner tracking chamber (ITC) and the time projection chamber (TPC). The ITC is a cylindrical drift chamber with eight axial wire layers with radii between 16 and 26 cm. The TPC measures up to 21 space points per track at radii between 40 and 171 cm, and also provides a measurement of the specific ionization energy loss ($\mathrm{d}E/\mathrm{d}x$) of each charged track. These three detectors form the tracking system, which is immersed in a 1.5 T axial magnetic field provided by a super-conducting solenoid. The combined tracking system yields a transverse-momentum resolution of $\sigma(p_T)/p_T = 6 \times 10^{-4} p_T(\mathrm{GeV}/c) \oplus 0.005$. The resolution of the three-dimensional impact parameter for tracks having two VDET hits can be parametrised as $\sigma = 25\ \mu\mathrm{m} + 95\mu\mathrm{m}/p$, ($p$ in GeV/c).

The electromagnetic calorimeter (ECAL) is a lead/wire chamber sandwich operated in proportional mode. The calorimeter is read out in projective towers that subtend typically $0.9^\circ \times 0.9^\circ$, segmented in three longitudinal sections. The hadron calorimeter (HCAL) uses the iron return yoke as absorber. Hadronic showers are sampled by 23 planes of streamer tubes, with analogue projective tower and digital hit pattern readouts. The HCAL is used in combination with two double layers of muon chambers outside the magnet for muon identification.

3 Selection of $B \to \ell\nu D^{(\star)}$ decays

A Monte Carlo simulation based on JETSET 7.4 [4] and tuned to ALEPH data [5, 6] has been used in order to extract resolution functions, acceptance corrections and background compositions. About five million $b\bar{b}$ events were simulated, and more than twice the data statistics of $q\bar{q}$ events. The present analysis uses $b\bar{b}$ events to determine the x_B^{wd} and x_B^{L} spectrum starting from observed x_B^{obs} spectra, and $q\bar{q}$ events to evaluate the non-$b\bar{b}$ component of the selected sample.

The decays $B \to \ell\nu D^{(\star)}$ are searched for in hadronic events, containing at least one lepton (electron or muon) identified using standard criteria [7]. The momentum cut used to define lepton candidates is $p > 2$ GeV/c for electrons and $p > 2.5$ GeV/c for muons. The transverse momentum p_T of the lepton with respect to the nearest jet, with the lepton excluded from the jet, is required to be larger than 1 GeV/c, which helps rejecting fake candidates and leptons not coming from direct decays of b hadrons. Both electron and muon candidates are required to have a measured $\mathrm{d}E/\mathrm{d}x$ compatible with the expected value.

Events are divided into two hemispheres by a plane perpendicular to the thrust axis; in each hemisphere containing a lepton a D meson reconstruction is attempted in the decay modes described in Table 1. At least two charged tracks from the D meson decay are required to have VDET hits, in order to ensure a good reconstruction of the D vertex position and to reject combinatorial background. Loose cuts are applied to track momenta, in order to minimise the bias in the B momentum distribution. Tracks are not considered as kaon candidates if their measured ionization is incompatible with the kaon hypothesis by more than three standard deviations. The charge of the kaon candidate is required to be the same as that of the lepton, as expected for semileptonic B meson decays.

Tracks assigned to a D meson decay are fitted to a common vertex, and the track combination is rejected if the χ^2 of the fit is larger than 20. If more than one combination fulfils this requirement for channels 3 and 4, the one with the smallest χ^2 is chosen. In channel 5, the π^0 closest in angle to the charged pion is selected and added to form the D^0.

For channels 1, 2 and 5, a soft pion $\pi_{\rm s}$ is added to the D candidate to form a $D^\star$ meson; the $\pi_{\rm s}$ momentum is required to be larger than 250 MeV/c and smaller than 3 GeV/c. The difference between the reconstructed $D^\star$ and D masses is required to be within 5 MeV/c^2 of its nominal value. In the case of multiple candidates in a given hemisphere, the track combination is chosen for which the reconstructed $(D^\star - D)$ mass difference is closest to the nominal value.

A vertex fit is performed using the D candidate and the lepton track, and again the combination of tracks is rejected if the χ^2 of the fit is larger than 20. The B vertex is required to lie between the interaction point, reconstructed event-by-event, and the D vertex.

Channels 3 and 4 are further enriched in signal events using harder cuts on the kaon; in addition a $\pi_{\rm s}$ veto is applied: if a track is found which is compatible with the reconstructed B vertex and the combination track-D candidate has a mass close to the mass of the $D^\star$, the candidate is discarded. This procedure reduces the overlap between channels at the permil level. Finally, tighter cuts on the reconstructed D mass and the χ^2 of the vertex fit are imposed.

The D mass spectra are shown in Fig. 1. The reconstructed D mass peaks are fitted in a region between 1.7 and 2.0 GeV/c^2 with a Gaussian and a linear component. Table 2 shows the chosen D mass windows, the number of reconstructed candidates and the fitted Gaussian fractions.

The fractions of the Gaussian components measured in the Monte Carlo are compatible

Channel	D window (MeV/c^2)	Events	Resolution (MeV/c^2)	Gaussian Fraction
$D^\star \to D^0\pi_{\rm s}$ $D^0 \to K\pi$	1864 ± 30	665	8.3	89 %
$D^\star \to D^0\pi_{\rm s}$ $D^0 \to K\pi\pi\pi$	1864 ± 30	388	6.2	69 %
$D^0 \to K\pi$	1864 ± 15	1079	8.4	81 %
$D \to K\pi\pi$	1869 ± 30	580	7.4	64 %
$D^\star \to D^0\pi_{\rm s}$ $D^0 \to K\pi\pi^0$	1864 ± 50	693	25	63 %

Table 2: For the five channels, the D mass window, the number of events in the window, the mass resolution and the Gaussian fraction.

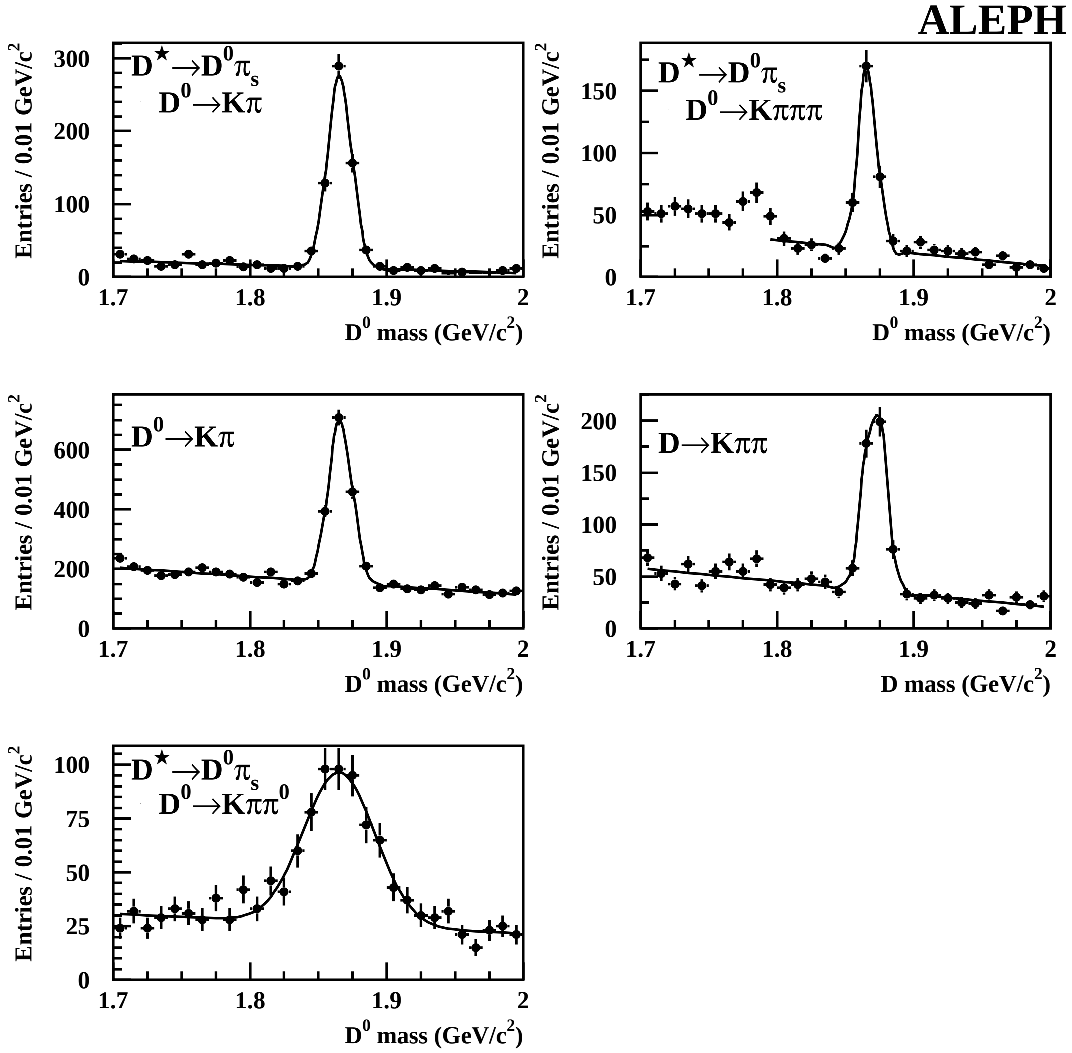

Figure 1: Reconstructed D mass peaks in the five channels. In the second channel the second peak at lower mass comes from the decay channel $D^0 \to K\pi\pi\pi\pi^0$ and is excluded from the fit.

with those in the data within statistical errors, while the widths are about $5-10\%$ smaller; this is taken into account in the evaluation of the systematic uncertainties.

4 B energy reconstruction

The scaled energy of the weakly-decaying $B \to \ell\nu D^{(\star)}$ hadron is estimated as

$$x_B^{\rm obs} = \frac{E_\ell + E_{D^{(\star)}} + E_\nu}{E_{\rm beam}} \quad . \tag{3}$$

The terms $E_{D^{(\star)}}$ and E_ℓ are provided by the direct reconstruction, while the neutrino energy E_ν is estimated from the missing energy in the hemisphere:

$$E_\nu = E_{\rm tot}^{\rm hemi} - E_{\rm vis}^{\rm hemi} \quad , \tag{4}$$

where $E_{\rm tot}^{\rm hemi}$ is estimated taking into account the measured mass in both hemispheres [8]:

$$E_{\rm tot}^{\rm hemi} = E_{\rm beam} + \frac{m_{\rm same}^2 - m_{\rm oppo}^2}{4E_{\rm beam}} \quad . \tag{5}$$

Both charged and neutral particles are used in Eqns. (4) and (5). In the lepton hemisphere neutral hadronic energy is expected to come only from fragmentation. Therefore, in order to avoid spurious calorimetric fluctuations, its contribution is taken into account only outside a cone of 10 degrees of half opening angle around each of the B meson decay products. Table 3 shows the resolution on x_B estimated on simulated $b\bar{b}$ events; the distributions are well described by two Gaussians, accounting for core and tails.

Channel		Core (%)	Core resolution	Tail resolution
$D^\star \to D^0\pi_\mathrm{s}$	$D^0 \to K\pi$	57	0.03	0.10
$D^\star \to D^0\pi_\mathrm{s}$	$D^0 \to K\pi\pi\pi$	54	0.04	0.12
	$D^0 \to K\pi$	61	0.05	0.15
	$D \to K\pi\pi$	65	0.05	0.15
$D^\star \to D^0\pi_\mathrm{s}$	$D^0 \to K\pi\pi^0$	57	0.04	0.11

Table 3: For the five channels the x_B resolution on simulated events. The resolution can be parametrised with two Gaussians, describing the core and the tails.

5 Unfolding methods

The scaled energy of the weakly-decaying B mesons, x_B^{obs}, is reconstructed in 20 bins between 0 and 1 with a variable width. In each bin, the non-$b\bar{b}$ background is estimated using the simulation, and subtracted from the spectrum. This amounts to about 2% of the events, concentrated mostly at low x_B^{obs}. The measured spectra after subtraction are shown in Fig. 2.

With these events two different kinds of analyses can be performed:

- a model-dependent analysis, in which different fragmentation models available in the literature are tuned to fit the observed spectra;
- a model-independent analysis, in which the shapes of x_B^{wd} and x_B^{L} are reconstructed by correcting the observed spectra for detector acceptance, resolution and missing particles.

5.1 Model-dependent analysis

Various fragmentation functions $D_b^H(z)$ are implemented in the Monte Carlo generator JETSET 7.4, which also simulates initial and final state photon radiation and hard gluon emission. The reconstructed spectra obtained from the simulated $b\bar{b}$ events are tuned to best reproduce the x_B^{obs} distribution observed in the data, by minimising the global χ^2. The following parametrisations for $D_b^H(z)$ are used:

$$\begin{aligned}
\text{Peterson } et\ al.\ [9]: \quad D_b^H(z) &\propto \frac{1}{z}\left(1-\frac{1}{z}-\frac{\epsilon_b}{1-z}\right)^{-2} \quad , \\
\text{Kartvelishvili } et\ al.\ [10]: \quad D_b^H(z) &\propto z^{\alpha_b}\,(1-z) \quad , \\
\text{Collins } et\ al.\ [11]: \quad D_b^H(z) &\propto \left(\frac{1-z}{z}+\frac{(2-z)\,\epsilon_b}{1-z}\right)\times \\
& \left(1+z^2\right)\left(1-\frac{1}{z}-\frac{\epsilon_b}{1-z}\right)^{-2} \quad .
\end{aligned}$$

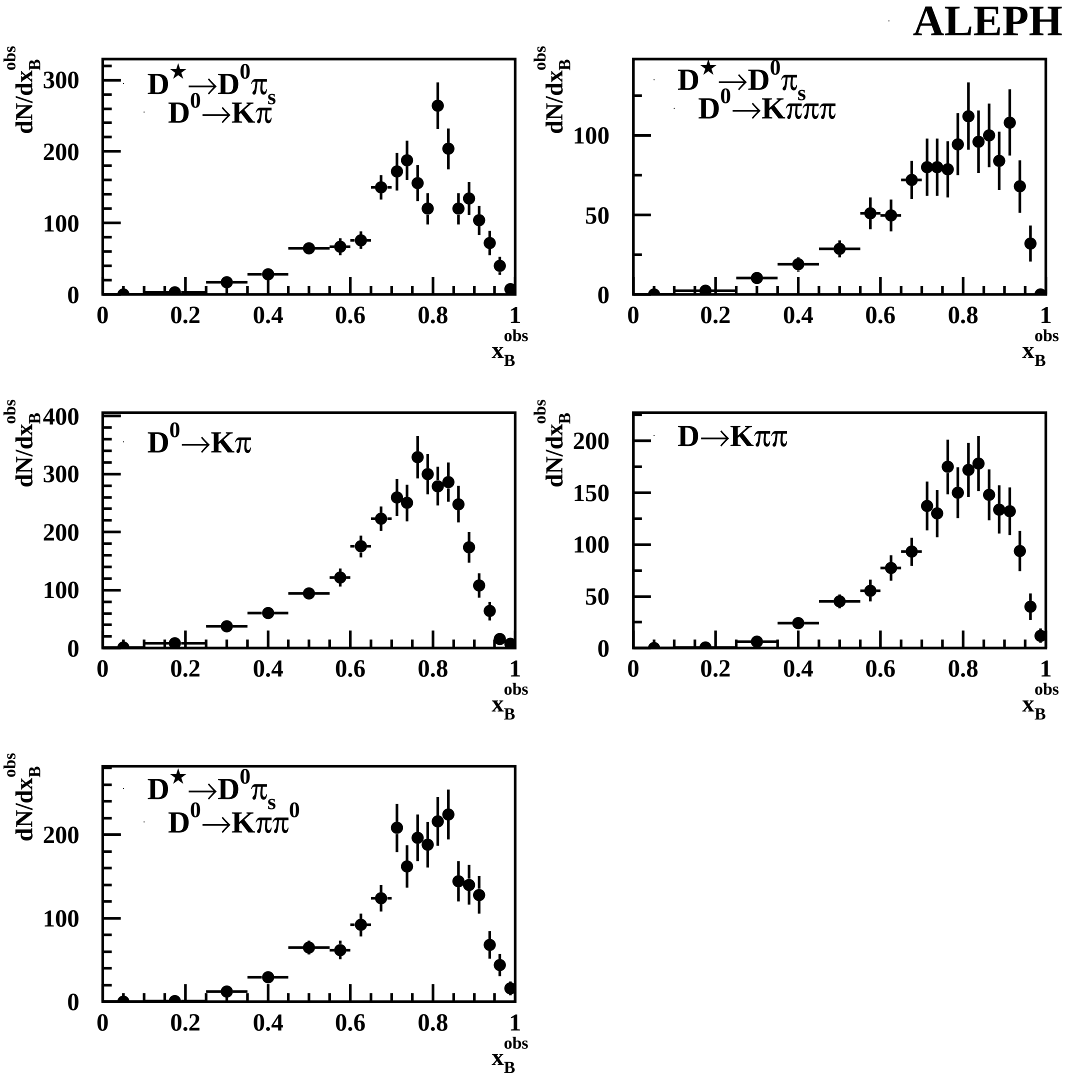

Figure 2: In the five channels, $x_B^{\rm obs}$ spectra, after non-$b\bar{b}$ background subtraction and before acceptance corrections.

The minimisation is performed with respect to the free parameter of each model, and the χ^2 is written as:

$$\chi^2 = \sum_{c=1}^{5} \sum_{i=1}^{20} \frac{\left[n_i^{\mathrm{DT}}(c) - n_i^{\mathrm{MC}}(c)\right]^2}{\left[\sigma_i^{\mathrm{DT}}(c)\right]^2 + \left[\sigma_i^{\mathrm{MC}}(c)\right]^2} \quad , \tag{6}$$

where c runs over the channels used, i runs over the x_B^{obs} bins defined as in Table 6, n^{DT} and n^{MC} are the number of candidates per channel and per bin observed in the data and expected from the Monte Carlo, normalised to the same number of entries. The quantities σ are defined as statistical uncertainties.

Table 4 shows the fitted values for the different model parameters, together with statistical and systematic uncertainties from the sources discussed in Section 6. Also shown are the values for the mean scaled energy.

Model	Fit results	Mean energies
Peterson [9]	$\epsilon_b = (31 \pm 3 \pm 5) \times 10^{-4}$ $\chi^2/N_{\mathrm{DOF}} = 117/94$	$\langle x_B^{\mathrm{wd}} \rangle = (700 \pm 4 \pm 5) \times 10^{-3}$ $\langle x_B^{\mathrm{L}} \rangle = (721 \pm 4 \pm 5) \times 10^{-3}$
Kartvelishvili [10]	$\alpha_\beta = 13.7 \pm 0.7 \pm 1.1$ $\chi^2/N_{\mathrm{DOF}} = 107/94$	$\langle x_B^{\mathrm{wd}} \rangle = (713 \pm 4 \pm 6) \times 10^{-3}$ $\langle x_B^{\mathrm{L}} \rangle = (734 \pm 4 \pm 6) \times 10^{-3}$
Collins [11]	$\epsilon_b = (185 \pm 25 \pm 41) \times 10^{-5}$ $\chi^2/N_{\mathrm{DOF}} = 181/94$	$\langle x_B^{\mathrm{wd}} \rangle = (681 \pm 4 \pm 5) \times 10^{-3}$ $\langle x_B^{\mathrm{L}} \rangle = (701 \pm 4 \pm 5) \times 10^{-3}$

Table 4: Fit results with different fragmentation models. The systematic errors account for the sources of uncertainties discussed in Section 6. The χ^2/N_{DOF} is calculated using statistical errors only.

The Kartvelishvili model describes the data slightly better than the Peterson model. The Collins model is clearly disfavoured.

5.2 Model-independent analysis

The x_B^{wd} and x_B^{L} spectra are obtained by correcting the observed x_B^{obs} spectra for acceptance, detector resolution and missing particles.

The normalised binned spectrum $f_i\left(x_B^{\mathrm{wd}}\right)$ can be obtained using the relation

$$f_i\left(x_B^{\mathrm{wd}}\right) = \frac{1}{T} \sum_{c=1}^{5} \frac{1}{\epsilon_i^{\mathrm{wd}}(c)} \sum_{j=1}^{20} G_{ij}^{\mathrm{wd}}(c)\, n_j^{\mathrm{DT}}(c) \quad , \tag{7}$$

where $\epsilon_i^{\mathrm{wd}}(c)$ is the acceptance correction in bin i for channel c; $n_j^{\mathrm{DT}}(c)$ is the number of reconstructed B mesons in the data for channel c, with a measured energy falling in bin j; $G_{ij}^{\mathrm{wd}}(c)$ is the resolution matrix that links mesons with x_B^{obs} in bin j and x_B^{wd} in bin i, for channel c; T is the normalisation factor defined by the condition $\sum_i f_i = 1$. A similar equation holds for the extraction of $f_i\left(x_B^{\mathrm{L}}\right)$, where the effect of the missing particles from $B^\star$ and $B^{\star\star}$ decays is folded in ϵ^{L} and G^{L}.

The acceptance corrections ϵ_i and the resolution matrix G_{ij} are taken from the simulation. The acceptance corrections show a different behaviour among the different channels; the two extreme situations are shown in Fig. 3. A dependence on the fragmentation function present in Monte Carlo is induced in the measured spectrum through G_{ij}; hence, the Monte Carlo used to calculate G_{ij} must be reweighted to the best estimate of $f_i\left(x_B^{\mathrm{wd}}\right)$ from data. This is done using an iterative procedure, calculating $f_i^N\left(x_B^{\mathrm{wd}}\right)$ using the G_{ij}^{N-1}

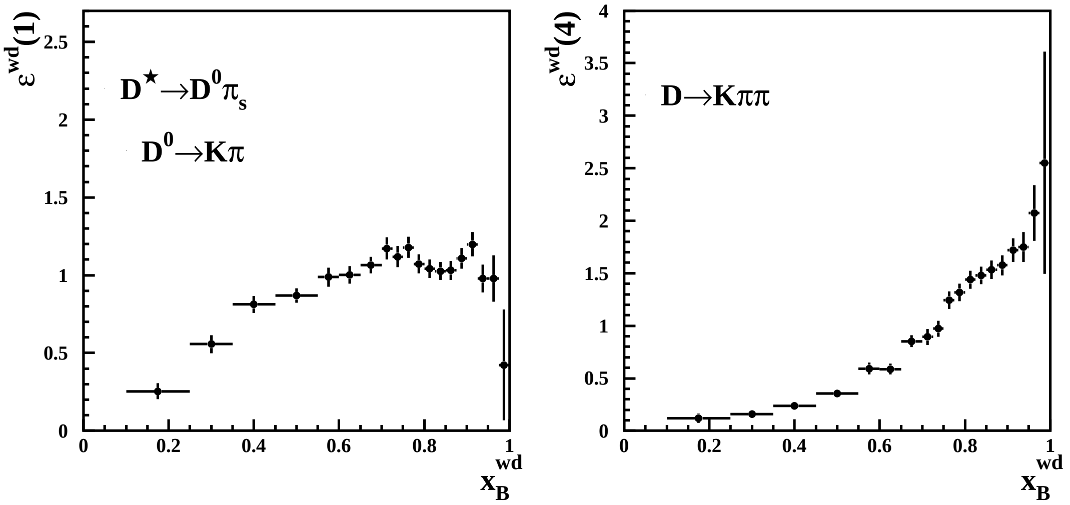

Figure 3: Acceptance corrections $\epsilon_i^{\mathrm{wd}}(c)$ for x_B^{wd}. The absolute scale is chosen as to conserve the total number of selected events for each channel. Only the distributions for channels 1 and 4 are shown, since they represent the extreme behaviours.

from Monte Carlo reweighted to $f_i^{N-1}\left(x_B^{\mathrm{wd}}\right)$. The weights $w_i \equiv f_i^{N-1}(\mathrm{DT})/f_i(\mathrm{MC})$ are applied to standard Monte Carlo events; to avoid fluctuations due to the limited statistics in data events, the distribution of the weights w_i is smoothed with a polynomial function. Possible systematic effects related to the smoothing are studied in Section 7.

The whole procedure is then repeated until the change in f_i in consecutive iterations is a small fraction of the statistical errors.

The statistical error matrix E_{ij} is calculated by repeating 20 × 5 analyses, varying in each of them the quantities $n_j^{\mathrm{DT}}(c)$ by one standard deviation:

$$E_{ij} = \sum_{c=1,5} \sum_{k=1,20} (f_i^{(ck)} - f_i^{\mathrm{STD}})(f_j^{(ck)} - f_j^{\mathrm{STD}}) \quad , \tag{8}$$

where $f_i^{(ck)}$ is the result of the convergence for f_i when $n_k^{\mathrm{DT}}(c)$ is varied by its statistical error, and f_i^{STD} the nominal result.

The results, together with the statistical and systematic errors, are given in Table 6. The full error matrices are shown in the Appendix.

From the binned spectra $f_i\left(x_B^{\mathrm{wd}}\right)$ the mean value is calculated as

$$\langle x_B^{\mathrm{wd}} \rangle = \sum_{i=1}^{20} x_i \, f_i\left(x_B^{\mathrm{wd}}\right) \quad , \tag{9}$$

where x_i is the central value of bin i. The bin size chosen is such that the deviation from linearity of the distribution within a bin is negligible.

The statistical error on $\langle x_B \rangle$ is calculated using the same procedure used as for f_i.

The results for $\langle x_B^{\mathrm{wd}} \rangle$ and $\langle x_B^{\mathrm{L}} \rangle$ are

$$\begin{aligned} \langle x_B^{\mathrm{wd}} \rangle &= 0.7163 \pm 0.0061\,(\mathrm{stat}) \quad , \\ \langle x_B^{\mathrm{L}} \rangle &= 0.7361 \pm 0.0063\,(\mathrm{stat}) \quad . \end{aligned}$$

Process	BR(%)
$B \to D\ell\nu$	1.95 ± 0.27
$B \to D^\star\ell\nu$	5.05 ± 0.25
$B \to D^{(\star)}X\ell\nu$	2.7 ± 0.7
with $B \to D_1\ell\nu$	0.63 ± 0.11
with $B \to D_2^\star\ell\nu$	0.23 ± 0.09
$b \to u\ell\nu$	0.15 ± 0.10
$\sum B \to \ell\nu X$	9.85 ± 0.80
Inclusive $B \to \ell\nu X$	10.18 ± 0.39

Table 5: Exclusive branching ratios for the $B \to \ell\nu X$ process [12, 13]. The sum is consistent with the measurement of the inclusive $B \to \ell\nu X$ rate.

6 Systematic errors

Possible systematic effects due to uncertainties on the physics parameters used in the Monte Carlo, limited accuracy in the simulation of the detector response, or effects intrinsic to the analysis method have been investigated.

The physics parameters used in the Monte Carlo simulation that are relevant for the analysis are adjusted to the most recent experimental measurements and varied within their estimated uncertainty by reweighting simulated events. The effect of the reweighting propagates to the results through the resolution matrix $G_{ij}(c)$ and the acceptance corrections $\epsilon_i(c)$, which are taken from the simulation. The differences from the standard results are taken as systematic errors.

The sources of uncertainty considered are:

- Semileptonic decays of B mesons.

  The current experimental knowledge [12, 13] of the semileptonic branching ratios of B mesons is summarised in Table 5. The sum of the exclusive (or semi-exclusive) rates is consistent within errors with the inclusive measurement of $\mathrm{BR}(B \to \ell\nu X)$.

  The analysis is not sensitive to the total $\mathrm{BR}(B \to \ell\nu X)$, but is affected by a change in the relative rates of the different components, since these contribute in a different way to the average acceptance corrections and resolution matrix.

  Six sources of systematic error are calculated using the values in Table 5:

  1. The inclusive $\mathrm{BR}(B \to D^{(\star)}X\ell\nu)$ is varied within its experimental error.

     $$\Delta\langle x_B^{\mathrm{wd}}\rangle = 0.0019 \quad \Delta\langle x_B^{\mathrm{L}}\rangle = 0.0020$$

  2. The rate for the narrow D_1 state is varied by its experimental error, while leaving the total $\mathrm{BR}(B \to D^{(\star)}X\ell\nu)$ at its central value.

     $$\Delta\langle x_B^{\mathrm{wd}}\rangle = 0.0001 \quad \Delta\langle x_B^{\mathrm{L}}\rangle = 0.0001$$

  3. The rate for the narrow $D_2^\star$ state is varied by its experimental error, while leaving the total $\mathrm{BR}(B \to D^{(\star)}X\ell\nu)$ at its central value.

     $$\Delta\langle x_B^{\mathrm{wd}}\rangle = 0.0001 \quad \Delta\langle x_B^{\mathrm{L}}\rangle = 0.0001$$

4. The rate of wide $D^{\star\star}$ states, not yet measured, is put to zero and compensated with non-resonant $D^{(\star)}\ell\nu\pi$ final states, thus leaving the total $\mathrm{BR}(B \to D^{(\star)}X\ell\nu)$ at its central value.

$$\Delta\langle x_B^{\mathrm{wd}}\rangle = 0.0017 \quad \Delta\langle x_B^{\mathrm{L}}\rangle = 0.0016$$

5. The $\mathrm{BR}(B \to D\ell\nu)$ is varied by its experimental error:

$$\Delta\langle x_B^{\mathrm{wd}}\rangle = 0.0008 \quad \Delta\langle x_B^{\mathrm{L}}\rangle = 0.0007$$

6. The $\mathrm{BR}(B \to D^{\star}\ell\nu)$ is varied by its experimental error:

$$\Delta\langle x_B^{\mathrm{wd}}\rangle = 0.0008 \quad \Delta\langle x_B^{\mathrm{L}}\rangle = 0.0008$$

- Missing particles from $B^{\star\star}$ production.

  When deriving the energy spectrum of the leading B meson, the correction due the energy carried away by the pion produced in the $B^{\star\star}$ decay enters in the resolution matrix and the acceptance corrections. The rate of $b \to B^{\star\star}$ is varied within its experimental error: $f_{B^{\star\star}} = 0.299 \pm 0.058$ [14, 15, 16], and the resulting systematic error is $\Delta\langle x_B^{\mathrm{L}}\rangle = 0.0025$. The weakly-decaying B meson spectrum is not affected by this source of uncertainty.

- Modelling of the $B^{\star\star}$ production.

  From spin counting, the relative rates of (B_1, $B_0^{\star}$, $B_1^{\star}$, $B_2^{\star}$) are predicted to be (3,1,3,5) [17]; changing this to (1,1,1,1) gives a systematic error of $\Delta\langle x_B^{\mathrm{L}}\rangle = 0.0004$.

- Production of $B^{\star}$ from b quarks.

  Due to the small mass difference between $B^{\star}$ and B mesons, the effect of $B^{\star}$ production in b quark fragmentation is found to be much smaller than for $B^{\star\star}$, and it is completely negligible for the present analysis.

The relevant sources of systematic uncertainties due to the detector simulation are identified to be:

- Neutrino energy reconstruction.

  The accuracy of the neutrino energy reconstruction is checked in hadronic events enriched in light primary quarks and in hadronic decays of $\tau\tau$ events. In the first sample, a “fake” neutrino is simulated by removing a charged particle from the reconstructed event; its energy is then reconstructed using Eqns. (4) and (5). The method can be applied both to data and Monte Carlo events, determining the bias between the reconstructed energy and the momentum measured with the tracking system. Such a bias is found to be reproduced by the Monte Carlo with a precision better than 50 MeV, for all momenta of the deleted track. In the second sample, where the event topology is much simpler, the energy of the “reconstructed” ν_τ is compared between data and Monte Carlo events. Also in this case the worst discrepancy observed is smaller than 50 MeV. This value is used as a conservative estimate of the systematic uncertainty on the neutrino energy, resulting in $\Delta\langle x_B^{\mathrm{wd}}\rangle = 0.0023$ and $\Delta\langle x_B^{\mathrm{L}}\rangle = 0.0023$.

- Vertexing and charm meson reconstruction.

  If the purity and the kinematic properties of the selected candidates are not well described by the simulation, the acceptance corrections and resolution matrices can be inadequate. In order to check for these effects, the distributions of the χ^2 probability for the reconstructed D vertices are compared, channel by channel, with the simulation. Small differences are observed, and the Monte Carlo distribution is reweighted in order to reproduce the data. The shift in the corrected average energy is taken as systematic uncertainty. The resulting error estimates are $\Delta\langle x_B^{\mathrm{wd}}\rangle = 0.0001$ and $\Delta\langle x_B^{\mathrm{L}}\rangle = 0.0001$.

  Furthermore, the reconstructed D mass distributions in data and Monte Carlo are compared. In simulated events the widths of the mass spectra are found to be $5-10\%$ smaller, while the fractions of the Gaussian components, estimated from a fit to the sidebands, are reproduced within their statistical error of about 5%. The mass cuts reported in Table 2 are adjusted in order to take into account both effects, taking the total shift in the extracted energy spectrum as systematic uncertainty. The resulting estimates are

$$\Delta\langle x_B^{\mathrm{wd}}\rangle\Big|_{\mathrm{width}} = 0.0011 \qquad \Delta\langle x_B^{\mathrm{L}}\rangle\Big|_{\mathrm{width}} = 0.0010 \quad ,$$
$$\Delta\langle x_B^{\mathrm{wd}}\rangle\Big|_{\mathrm{purity}} = 0.0021 \qquad \Delta\langle x_B^{\mathrm{L}}\rangle\Big|_{\mathrm{purity}} = 0.0021 \quad .$$

Possible systematic effects related to the analysis procedure are:

- Background subtraction.

  As previously explained, a bin-by-bin subtraction of candidates not coming from $b\bar{b}$ events is performed before deriving the B meson energy spectra. The efficiency for this kind of background has been extracted directly from data events, which have been enriched in background events by selecting wrong sign candidates. It is found to be compatible with Monte Carlo simulation within the statistical error of about 25%. The background is varied within this range and the systematic errors associated are $\Delta\langle x_B^{\mathrm{wd}}\rangle = 0.0021$ and $\Delta\langle x_B^{\mathrm{L}}\rangle = 0.0022$.

- Monte Carlo statistics.

  Statistics of simulated events are larger than for data events by a factor of 5. In order to evaluate the related uncertainty, the acceptance corrections $\epsilon_i(c)$ and the matrix elements $G_{ij}(c)$ are varied randomly by their statistical error in a series of toy experiments. The scatter of the results for $\langle x_B^{\mathrm{wd}}\rangle$ and $\langle x_B^{\mathrm{L}}\rangle$ is taken as an estimate of the uncertainty due to the limited Monte Carlo statistics, yielding $\Delta\langle x_B^{\mathrm{wd}}\rangle = 0.0029$ and $\Delta\langle x_B^{\mathrm{L}}\rangle = 0.0031$.

Adding in quadrature all the systematic contributions, the final results are:

$$\begin{aligned}\langle x_B^{\mathrm{wd}}\rangle &= 0.7163 \pm 0.0061\,(\mathrm{stat}) \pm 0.0056\,(\mathrm{syst}) \quad ,\\ \langle x_B^{\mathrm{L}}\rangle &= 0.7361 \pm 0.0063\,(\mathrm{stat}) \pm 0.0063\,(\mathrm{syst}) \quad .\end{aligned}$$

The bin-by-bin results for the measured spectra, with the total systematic uncertainties, are shown in Table 6, while the statistical and total error matrices are reported in the Appendix. The spectra are also shown in Fig. 4, where they are compared with the Monte Carlo predictions from different fragmentation models, with the free parameters fitted to the data.

The models of Peterson and Kartvelishvili give the best agreement with the data, and are compared with the x_B^{wd} measurement in Fig. 5.

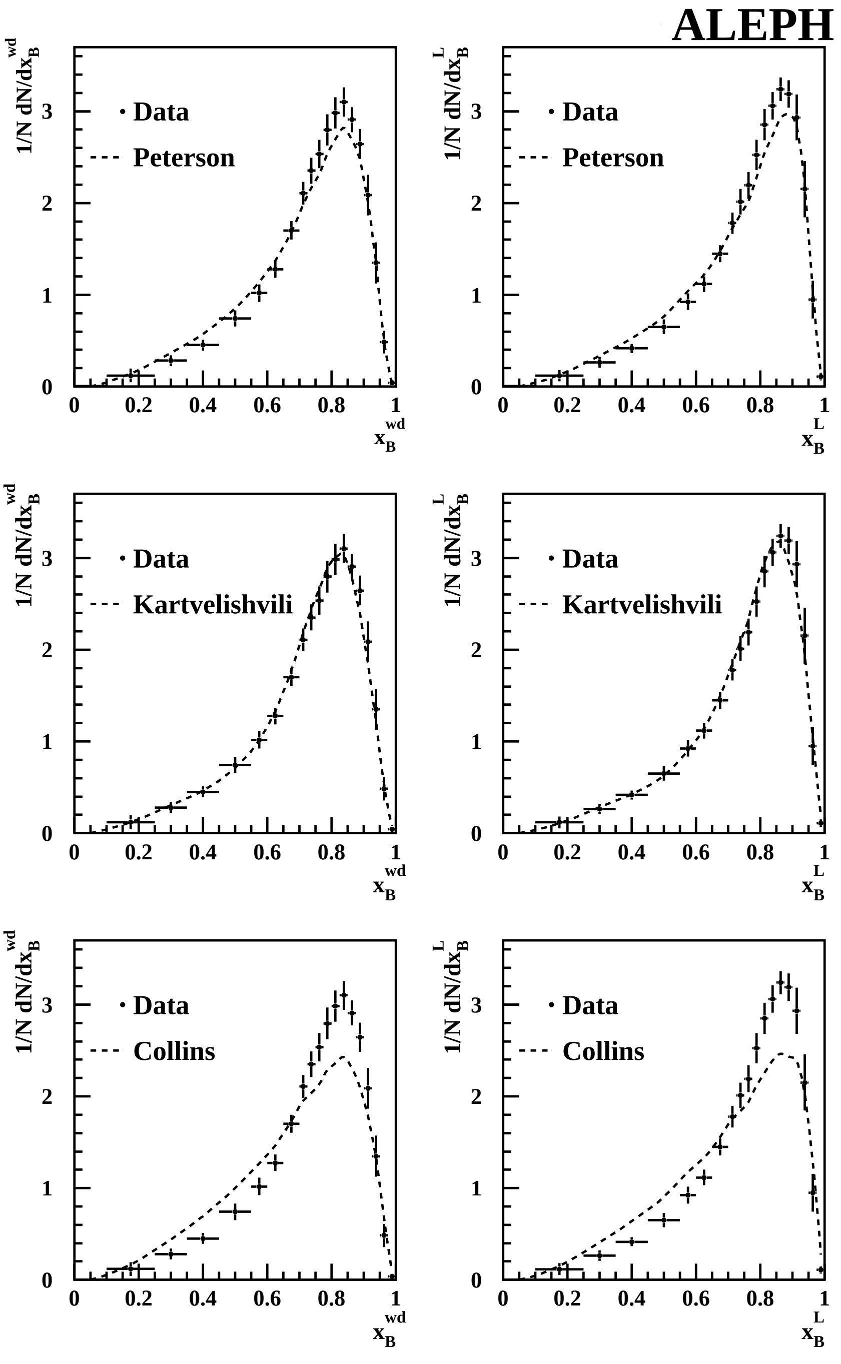

Figure 4: Scaled energy of the leading and weakly-decaying B meson, as reconstructed from data. The best-fit distributions for the Peterson model, the Kartvelishvili model, and the Collins model are superimposed. For the data, the bin-to-bin errors are highly correlated, as shown in the error matrices in the Appendix.

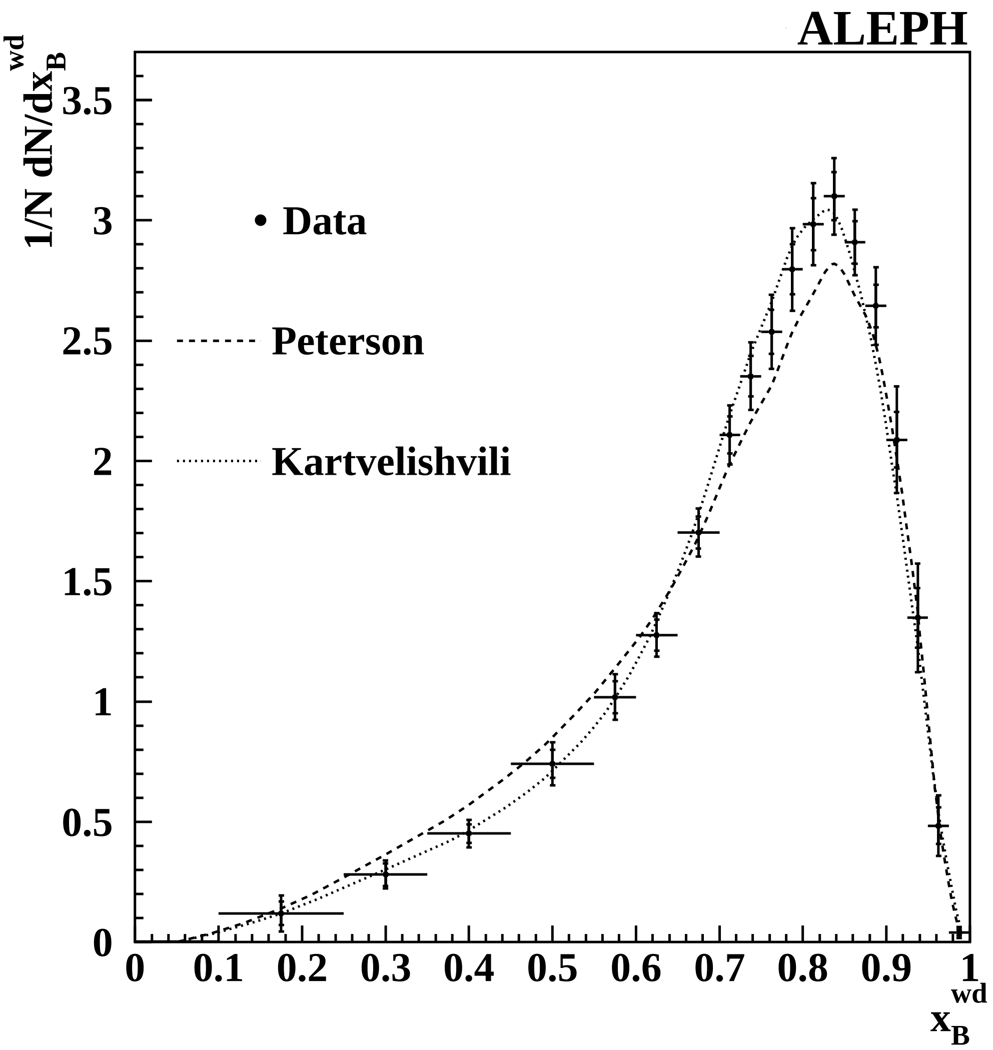

Figure 5: Scaled energy of the weakly-decaying B meson, as reconstructed from data. The inner error bars represent statistical errors, the larger ones the total uncertainties. The best-fit distributions for the Peterson model and the Kartvelishvili model are superimposed. For the data, the bin-to-bin errors are highly correlated, as shown in the error matrices in the Appendix.

Bin	x_B Range	$f_i\left(x_B^{\mathrm{wd}}\right)$	$f_i\left(x_B^{\mathrm{L}}\right)$
1	0. – 0.1	–	–
2	0.1 – 0.25	$17.9 \pm 7.3 \pm 8.6$	$17.6 \pm 7.0 \pm 6.4$
3	0.25 – 0.35	$28.1 \pm 4.7 \pm 3.5$	$26.4 \pm 4.6 \pm 3.6$
4	0.35 – 0.45	$45.1 \pm 3.9 \pm 4.3$	$41.6 \pm 3.8 \pm 2.9$
5	0.45 – 0.55	$74.1 \pm 5.9 \pm 6.6$	$65.1 \pm 5.5 \pm 5.7$
6	0.55 – 0.6	$50.9 \pm 3.3 \pm 3.4$	$46.2 \pm 3.1 \pm 3.3$
7	0.6 – 0.65	$63.8 \pm 3.2 \pm 3.2$	$55.8 \pm 2.9 \pm 3.0$
8	0.65 – 0.7	$85.1 \pm 3.3 \pm 3.7$	$72.4 \pm 2.9 \pm 3.6$
9	0.7 – 0.725	$52.7 \pm 1.9 \pm 2.4$	$44.5 \pm 1.7 \pm 2.4$
10	0.725 – 0.75	$58.8 \pm 2.1 \pm 2.8$	$50.3 \pm 1.9 \pm 2.9$
11	0.75 – 0.775	$63.4 \pm 2.3 \pm 3.1$	$54.8 \pm 2.1 \pm 3.0$
12	0.775 – 0.8	$69.9 \pm 2.6 \pm 3.4$	$63.1 \pm 2.5 \pm 3.3$
13	0.8 – 0.825	$74.6 \pm 2.7 \pm 3.3$	$71.3 \pm 2.7 \pm 3.3$
14	0.825 – 0.85	$77.5 \pm 2.5 \pm 3.1$	$76.5 \pm 2.6 \pm 2.7$
15	0.85 – 0.875	$72.7 \pm 2.2 \pm 2.6$	$81.0 \pm 2.3 \pm 2.2$
16	0.875 – 0.9	$66.1 \pm 2.2 \pm 3.4$	$79.7 \pm 2.1 \pm 3.1$
17	0.9 – 0.925	$52.2 \pm 2.9 \pm 4.7$	$73.3 \pm 3.0 \pm 5.5$
18	0.925 – 0.95	$33.7 \pm 3.1 \pm 4.7$	$53.8 \pm 3.9 \pm 6.6$
19	0.95 – 0.975	$12.1 \pm 1.9 \pm 2.5$	$23.7 \pm 2.8 \pm 4.3$
20	0.975 – 1.	$1.0 \pm 0.3 \pm 0.5$	$2.7 \pm 0.6 \pm 0.8$

Table 6: The extracted spectra for the weakly-decaying B meson and the leading B meson. All numbers are given in units of 10^{-3}.

7 Systematic checks

Possible systematic effects intrinsic to the analysis method are checked by measuring the energy spectra in a sample of 8 million simulated $q\bar{q}$ events. The average values for the scaled energies of the weakly-decaying and leading B mesons are measured to be:

$$\begin{aligned} \langle x_B^{\mathrm{L}} \rangle_{\mathrm{MC}} &= 0.711 \pm 0.005\,(\mathrm{stat}) \quad , \\ \langle x_B^{\mathrm{wd}} \rangle_{\mathrm{MC}} &= 0.692 \pm 0.005\,(\mathrm{stat}) \quad , \end{aligned}$$

which compare well with the true values:

$$\begin{aligned} \langle x_B^{\mathrm{L}} \rangle_{\mathrm{MC}}^{\mathrm{true}} &= 0.712 \quad , \\ \langle x_B^{\mathrm{wd}} \rangle_{\mathrm{MC}}^{\mathrm{true}} &= 0.692 \quad . \end{aligned}$$

Electron and muon identification are affected by different sources of background, and the selection efficiencies and purities have a different dependence upon the track kinematics and isolation. It is therefore interesting to perform the analysis using separately events with electron candidates or muon candidates. Consistent results within uncorrelated errors are found:

$$\begin{aligned} \langle x_B^{\mathrm{wd}} \rangle_{\mathrm{electrons}} &= 0.724 \pm 0.010 \quad , \quad \langle x_B^{\mathrm{L}} \rangle_{\mathrm{electrons}} = 0.743 \pm 0.010 \quad , \\ \langle x_B^{\mathrm{wd}} \rangle_{\mathrm{muons}} &= 0.700 \pm 0.014 \quad , \quad \langle x_B^{\mathrm{L}} \rangle_{\mathrm{muons}} = 0.720 \pm 0.014 \quad . \end{aligned} \tag{10}$$

The acceptance corrections for the five channels are significantly different (Fig. 3) and the same is true for the resolution matrices. An inaccurate description of these inputs would easily lead to incompatible results among the different channels. This is checked by performing the analysis separately in the five sub-samples. The results, reported in Table 7, are compatible within uncorrelated uncertainties.

Channel	$\langle x_B^{\mathrm{wd}} \rangle$	$\langle x_B^{\mathrm{L}} \rangle$
1	0.700 ± 0.015	0.720 ± 0.016
2	0.700 ± 0.020	0.720 ± 0.022
3	0.714 ± 0.012	0.733 ± 0.013
4	0.720 ± 0.019	0.740 ± 0.019
5	0.738 ± 0.012	0.755 ± 0.013

Table 7: Results using the five channels separately. The errors are uncorrelated.

It has been checked that the results are independent of the choice of fragmentation functions in the Monte Carlo sample used to estimate the resolution matrix G_{ij} and the acceptances ϵ_i.

As explained in Section 5.2, the weights applied to reweight G_{ij} to a given fragmentation function are smoothed with a polynomial function to reduce the bin-to-bin fluctuations. However, the values for the mean scaled energies move by a small fraction of the statistical errors when such smoothing is not applied, and the total statistical errors remain nearly constant:

$$\langle x_B^{\mathrm{wd}} \rangle = 0.7177 \pm 0.0060 \quad , \quad \langle x_B^{\mathrm{L}} \rangle = 0.7370 \pm 0.0065 \quad . \tag{11}$$

Heavy flavoured hadrons originating from gluon splitting $g \rightarrow b\bar{b}$ have an energy much lower than hadrons coming from primary b quarks. A check on Monte Carlo events shows that the contribution of such events is negligible.

The analysis uses a binned representation of the fragmentation functions to compensate the relatively small statistical sample in the data. The binning chosen must not introduce biases in the measured values nor should it affect the statistical errors. This is checked by performing a number of analyses in which the binning is varied randomly around the standard one. Both the central values and the statistical uncertainties are stable.

8 Conclusions

Using the data collected by the ALEPH experiment at and around the Z resonance in the years 1991–1995, about 3400 semileptonic B^0 and $B^{\pm}$ decays have been selected. The scaled energy spectra of weakly-decaying and leading B mesons have been reconstructed, and their mean values were found to be:

$$\begin{aligned} \langle x_B^{\mathrm{wd}} \rangle &= 0.7163 \pm 0.0061\,(\mathrm{stat}) \pm 0.0056\,(\mathrm{syst}) \quad , \\ \langle x_B^{\mathrm{L}} \rangle &= 0.7361 \pm 0.0063\,(\mathrm{stat}) \pm 0.0063\,(\mathrm{syst}) \quad . \end{aligned}$$

The observed spectra have been compared with the prediction of JETSET 7.4 using different fragmentation models. The models of Peterson *et al.* [9] and Kartvelishvili *et al.* [10] give a reasonable description of the data while the Collins *et al.* [11] model is clearly disfavoured.

This measurement supersedes a previous analysis from ALEPH [18], which used a different method and smaller statistics.

The present result is compatible with the published results using b hadrons from L3 [19], OPAL [20] and SLD [21], and using B mesons from OPAL [22].

9 Acknowledgements

We wish to thank our colleagues in the CERN accelerator divisions for the successful operation of LEP. We are indebted to the engineers and technicians in all our institutions for their contribution to the excellent performance of ALEPH. Those of us from non-member countries thank CERN for its hospitality.

A Appendix

Tables 8 and 9 show the statistical and total error matrices for $x_B^{\rm wd}$; Tables 10 and 11 give the same information for $x_B^{\rm L}$.

References

[1] ALEPH Collaboration, *"A study of the decay width difference in the B_s^0 - $\bar{B}_s^0$ system using $\phi\phi$ correlations"*, Phys. Lett. **B486** (2000) 286.

[2] ALEPH Collaboration, *"ALEPH: a detector for electron-positron annihilations at LEP"*, Nucl. Instr. Meth. **A294** (1990) 121.

[3] ALEPH Collaboration *"Performance of the ALEPH detector at LEP"*, Nucl. Instr. Meth. **A360** (1995) 481.

[4] T. Sjöstrand, Comp. Phys. Comm. **82** (1994) 74.

[5] ALEPH Collaboration, *"Heavy flavour production and decay with prompt leptons in the ALEPH detector"*, Z. Phys. **C62** (1994) 179.

[6] ALEPH Collaboration, *"Studies of Quantum Chromodynamics with the ALEPH detector"*, Phys. Rep. **294** (1998) 1.

[7] ALEPH Collaboration, *"Heavy quark tagging with leptons in the ALEPH detector"*, Nucl. Instr. Meth. **A346** (1994) 461.

[8] ALEPH Collaboration, *"Measurement of the B_s^0 lifetime"*, Phys. Lett. **B322** (1994) 275.

[9] C. Peterson, D. Schlatter, I. Schmitt and P.M. Zerwas, Phys. Rev. **D27** (1983) 105.

[10] V. G. Kartvelishvili, A.K. Likehoded and V.A. Petrov, Phys. Lett. **B78** (1978) 615.

[11] P. Collins and T. Spiller, J. Phys. **G11** (1985) 1289.

[12] Particle Data Group, D.E. Groom *et al.*, Eur. Phys. J. **C15** (2000) 1.

bin	2	3	4	5	6	7	8	9	10	11	12	13	14	15	16	17	18	19	20
2	53.	28.	−3.	−31.	−18.	−15.	−9.	−1.	2.	5.	7.	7.	6.	2.	−3.	−9.	−12.	−8.	−1.
3	28.	22.	8.	−10.	−10.	−11.	−10.	−4.	−3.	−1.	0.	1.	1.	1.	−1.	−3.	−4.	−3.	0.
4	−3.	8.	15.	14.	3.	−1.	−6.	−5.	−6.	−7.	−7.	−7.	−5.	−3.	0.	3.	4.	3.	1.
5	−31.	−10.	14.	35.	17.	12.	3.	−3.	−6.	−9.	−12.	−13.	−12.	−8.	−2.	6.	10.	7.	1.
6	−18.	−10.	3.	17.	11.	10.	6.	1.	−1.	−3.	−5.	−6.	−6.	−5.	−2.	1.	4.	3.	1.
7	−15.	−11.	−1.	12.	10.	10.	9.	3.	1.	−1.	−2.	−4.	−5.	−5.	−3.	−1.	1.	2.	0.
8	−9.	−10.	−6.	3.	6.	9.	11.	5.	4.	3.	2.	0.	−2.	−3.	−4.	−4.	−3.	−1.	0.
9	−1.	−4.	−5.	−3.	1.	3.	5.	4.	4.	3.	3.	2.	1.	−1.	−2.	−3.	−3.	−2.	0.
10	2.	−3.	−6.	−6.	−1.	1.	4.	4.	5.	5.	5.	4.	2.	0.	−2.	−4.	−5.	−3.	0.
11	5.	−1.	−7.	−9.	−3.	−1.	3.	3.	5.	6.	6.	5.	4.	1.	−2.	−4.	−5.	−3.	−1.
12	7.	0.	−7.	−12.	−5.	−2.	2.	3.	5.	6.	7.	7.	5.	2.	−1.	−4.	−6.	−4.	−1.
13	7.	1.	−7.	−13.	−6.	−4.	0.	2.	4.	5.	7.	7.	6.	4.	0.	−3.	−5.	−4.	−1.
14	6.	1.	−5.	−12.	−6.	−5.	−2.	1.	2.	4.	5.	6.	6.	5.	2.	−1.	−3.	−3.	0.
15	2.	1.	−3.	−8.	−5.	−5.	−3.	−1.	0.	1.	2.	4.	5.	5.	4.	2.	0.	−1.	0.
16	−3.	−1.	0.	−2.	−2.	−3.	−4.	−2.	−2.	−2.	−1.	0.	2.	4.	5.	5.	4.	2.	0.
17	−9.	−3.	3.	6.	1.	−1.	−4.	−3.	−4.	−4.	−4.	−3.	−1.	2.	5.	8.	8.	5.	1.
18	−12.	−4.	4.	10.	4.	1.	−3.	−3.	−5.	−5.	−6.	−5.	−3.	0.	4.	8.	10.	6.	1.
19	−8.	−3.	3.	7.	3.	2.	−1.	−2.	−3.	−3.	−4.	−4.	−3.	−1.	2.	5.	6.	4.	1.
20	−1.	0.	1.	1.	1.	0.	0.	0.	0.	−1.	−1.	−1.	0.	0.	0.	1.	1.	1.	0.

Table 8: Statistical error matrix for x_B^{wd}. All the numbers are in units of 10^{-6}.

bin	2	3	4	5	6	7	8	9	10	11	12	13	14	15	16	17	18	19	20
2	127.	42.	−28.	−72.	−32.	−18.	1.	10.	14.	18.	19.	15.	7.	−3.	−17.	−30.	−31.	−18.	−3.
3	42.	34.	10.	−23.	−18.	−18.	−13.	−3.	0.	3.	6.	7.	6.	3.	−3.	−10.	−13.	−8.	−2.
4	−28.	10.	34.	33.	7.	−2.	−14.	−11.	−13.	−13.	−13.	−10.	−7.	−1.	4.	9.	9.	6.	1.
5	−72.	−23.	33.	79.	37.	24.	1.	−11.	−19.	−25.	−30.	−30.	−25.	−14.	3.	21.	29.	18.	3.
6	−32.	−18.	7.	37.	22.	19.	10.	−1.	−5.	−10.	−13.	−15.	−15.	−10.	−3.	6.	12.	8.	2.
7	−18.	−18.	−2.	24.	19.	21.	17.	5.	1.	−3.	−7.	−10.	−13.	−11.	−8.	−2.	3.	3.	1.
8	1.	−13.	−14.	1.	10.	17.	25.	13.	11.	9.	5.	0.	−6.	−11.	−15.	−16.	−12.	−5.	−1.
9	10.	−3.	−11.	−11.	−1.	5.	13.	9.	10.	10.	9.	6.	1.	−3.	−9.	−13.	−13.	−7.	−1.
10	14.	0.	−13.	−19.	−5.	1.	11.	10.	12.	13.	13.	10.	5.	−1.	−9.	−16.	−16.	−9.	−2.
11	18.	3.	−13.	−25.	−10.	−3.	9.	10.	13.	15.	16.	14.	9.	2.	−8.	−17.	−19.	−11.	−2.
12	19.	6.	−13.	−30.	−13.	−7.	5.	9.	13.	16.	18.	17.	13.	5.	−6.	−17.	−20.	−12.	−2.
13	15.	7.	−10.	−30.	−15.	−10.	0.	6.	10.	14.	17.	18.	15.	8.	−2.	−13.	−17.	−10.	−2.
14	7.	6.	−7.	−25.	−15.	−13.	−6.	1.	5.	9.	13.	15.	16.	11.	4.	−5.	−10.	−7.	−1.
15	−3.	3.	−1.	−14.	−10.	−11.	−11.	−3.	−1.	2.	5.	8.	11.	11.	10.	6.	1.	−1.	0.
16	−17.	−3.	4.	3.	−3.	−8.	−15.	−9.	−9.	−8.	−6.	−2.	4.	10.	17.	19.	16.	8.	1.
17	−30.	−10.	9.	21.	6.	−2.	−16.	−13.	−16.	−17.	−17.	−13.	−5.	6.	19.	30.	30.	16.	3.
18	−31.	−13.	9.	29.	12.	3.	−12.	−13.	−16.	−19.	−20.	−17.	−10.	1.	16.	30.	32.	17.	3.
19	−18.	−8.	6.	18.	8.	3.	−5.	−7.	−9.	−11.	−12.	−10.	−7.	−1.	8.	16.	17.	10.	2.
20	−3.	−2.	1.	3.	2.	1.	−1.	−1.	−2.	−2.	−2.	−2.	−1.	0.	1.	3.	3.	2.	0.

Table 9: Total error matrix for x_B^{wd}. All the numbers are in units of 10^{-6}.

bin	2	3	4	5	6	7	8	9	10	11	12	13	14	15	16	17	18	19	20
2	49.	28.	0.	−26.	−17.	−14.	−9.	−2.	1.	3.	6.	7.	7.	5.	−1.	−8.	−14.	−11.	−2.
3	28.	21.	8.	−8.	−9.	−9.	−9.	−4.	−3.	−2.	−1.	0.	1.	0.	−1.	−3.	−5.	−4.	−1.
4	0.	8.	14.	13.	3.	0.	−5.	−4.	−5.	−6.	−7.	−7.	−7.	−5.	−2.	1.	4.	4.	1.
5	−26.	−8.	13.	30.	15.	11.	4.	−2.	−5.	−7.	−10.	−12.	−12.	−10.	−4.	3.	10.	9.	2.
6	−17.	−9.	3.	15.	10.	8.	5.	1.	−1.	−2.	−4.	−5.	−6.	−5.	−3.	0.	4.	4.	1.
7	−14.	−9.	0.	11.	8.	8.	7.	2.	1.	0.	−2.	−3.	−4.	−4.	−3.	−1.	1.	2.	0.
8	−9.	−9.	−5.	4.	5.	7.	9.	4.	4.	3.	2.	1.	−1.	−2.	−3.	−4.	−3.	−2.	0.
9	−2.	−4.	−4.	−2.	1.	2.	4.	3.	3.	3.	3.	2.	1.	0.	−2.	−3.	−4.	−3.	−1.
10	1.	−3.	−5.	−5.	−1.	1.	4.	3.	4.	4.	4.	4.	3.	1.	−1.	−4.	−5.	−4.	−1.
11	3.	−2.	−6.	−7.	−2.	0.	3.	3.	4.	5.	5.	5.	4.	2.	−1.	−4.	−6.	−5.	−1.
12	6.	−1.	−7.	−10.	−4.	−2.	2.	3.	4.	5.	6.	7.	6.	4.	0.	−4.	−7.	−6.	−1.
13	7.	0.	−7.	−12.	−5.	−3.	1.	2.	4.	5.	7.	7.	7.	5.	1.	−4.	−7.	−6.	−1.
14	7.	1.	−7.	−12.	−6.	−4.	−1.	1.	3.	4.	6.	7.	7.	5.	2.	−2.	−6.	−5.	−1.
15	5.	0.	−5.	−10.	−5.	−4.	−2.	0.	1.	2.	4.	5.	5.	5.	3.	1.	−2.	−2.	−1.
16	−1.	−1.	−2.	−4.	−3.	−3.	−3.	−2.	−1.	−1.	0.	1.	2.	3.	4.	5.	4.	2.	0.
17	−8.	−3.	1.	3.	0.	−1.	−4.	−3.	−4.	−4.	−4.	−4.	−2.	1.	5.	9.	11.	7.	1.
18	−14.	−5.	4.	10.	4.	1.	−3.	−4.	−5.	−6.	−7.	−7.	−6.	−2.	4.	11.	15.	10.	2.
19	−11.	−4.	4.	9.	4.	2.	−2.	−3.	−4.	−5.	−6.	−6.	−5.	−2.	2.	7.	10.	8.	2.
20	−2.	−1.	1.	2.	1.	0.	0.	−1.	−1.	−1.	−1.	−1.	−1.	−1.	0.	1.	2.	2.	0.

Table 10: Statistical error matrix for x_B^{L}. All the numbers are in units of 10^{-6}.

bin	2	3	4	5	6	7	8	9	10	11	12	13	14	15	16	17	18	19	20
2	90.	48.	−6.	−55.	−33.	−26.	−12.	2.	9.	14.	19.	22.	20.	11.	−2.	−26.	−40.	−29.	−6.
3	48.	34.	9.	−19.	−17.	−16.	−12.	−4.	−2.	1.	3.	5.	5.	2.	−1.	−10.	−14.	−11.	−2.
4	−6.	9.	23.	25.	7.	2.	−7.	−8.	−10.	−12.	−13.	−14.	−13.	−9.	−3.	6.	12.	9.	2.
5	−55.	−19.	25.	62.	32.	23.	7.	−5.	−12.	−17.	−23.	−27.	−26.	−20.	−9.	12.	27.	21.	5.
6	−33.	−17.	7.	32.	20.	17.	11.	2.	−2.	−5.	−9.	−12.	−13.	−11.	−8.	1.	8.	8.	2.
7	−26.	−16.	2.	23.	17.	17.	15.	6.	3.	1.	−2.	−5.	−8.	−10.	−10.	−6.	−2.	1.	1.
8	−12.	−12.	−7.	7.	11.	15.	22.	12.	12.	11.	9.	6.	0.	−6.	−13.	−20.	−21.	−12.	−2.
9	2.	−4.	−8.	−5.	2.	6.	12.	9.	10.	10.	10.	8.	4.	−1.	−8.	−15.	−18.	−11.	−2.
10	9.	−2.	−10.	−12.	−2.	3.	12.	10.	12.	12.	13.	12.	8.	1.	−7.	−18.	−23.	−15.	−3.
11	14.	1.	−12.	−17.	−5.	1.	11.	10.	12.	14.	15.	14.	10.	3.	−6.	−19.	−25.	−17.	−3.
12	19.	3.	−13.	−23.	−9.	−2.	9.	10.	13.	15.	17.	17.	13.	6.	−5.	−20.	−28.	−19.	−4.
13	22.	5.	−14.	−27.	−12.	−5.	6.	8.	12.	14.	17.	19.	15.	8.	−2.	−18.	−26.	−19.	−4.
14	20.	5.	−13.	−26.	−13.	−8.	0.	4.	8.	10.	13.	15.	14.	10.	3.	−9.	−17.	−13.	−3.
15	11.	2.	−9.	−20.	−11.	−10.	−6.	−1.	1.	3.	6.	8.	10.	10.	8.	3.	−2.	−3.	−1.
16	−2.	−1.	−3.	−9.	−8.	−10.	−13.	−8.	−7.	−6.	−5.	−2.	3.	8.	14.	19.	19.	10.	2.
17	−26.	−10.	6.	12.	1.	−6.	−20.	−15.	−18.	−19.	−20.	−18.	−9.	3.	19.	39.	46.	30.	5.
18	−40.	−14.	12.	27.	8.	−2.	−21.	−18.	−23.	−25.	−28.	−26.	−17.	−2.	19.	46.	59.	39.	7.
19	−29.	−11.	9.	21.	8.	1.	−12.	−11.	−15.	−17.	−19.	−19.	−13.	−3.	10.	30.	39.	27.	5.
20	−6.	−2.	2.	5.	2.	1.	−2.	−2.	−3.	−3.	−4.	−4.	−3.	−1.	2.	5.	7.	5.	1.

Table 11: Total error matrix for x_B^{L}. All the numbers are in units of 10^{-6}.

[13] LEP, SLD Collaborations, *“Combined results on b-hadron production rates, lifetimes, oscillations and semileptonic decays”*, CERN EP/2000-096 (Contributed paper to 1999 summer conference).

[14] CDF Collaboration, *“Observation of Orbitally Excited B Mesons in* $p\bar{p}$ *Collisions at* $\sqrt{s} = 1.8\ TeV$*”*, Submitted to Phys. Rev. D.

[15] ALEPH Collaboration, *“Resonant structure and flavour tagging in the* $B^{\pm}$ *system using fully reconstructed B decays”*, Phys. Lett. **B425** (1998) 215.

[16] DELPHI Collaboration, *“Observation of Orbitally Excited B Mesons ”*, Phys. Lett. **B 345** (1995) 598.

[17] N. Isgur and M.B. Wise, Phys. Lett. **B232** (1989) 13.

[18] ALEPH Collaboration, *“Measurement of the effective b quark fragmentation function at the Z resonance”*, Phys. Lett. **B357** (1995) 699.

[19] L3 Collaboration, *“Measurement of* $Z^0 \rightarrow b\bar{b}$ *Decays and the Semileptonic Branching Ratio* $Br(b \rightarrow l + X)$ *”*, Phys. Lett. **B 261** (1991) 177.

[20] OPAL Collaboration, *“Measurements of inclusive semileptonic branching fractions of b hadrons in Z decays”*, Eur. Phys. J. **C13** (2000) 225.

[21] SLD Collaboration. *“Precise measurement of the b quark fragmentation functions in* Z^0 *boson decays”*, Phys. Rev. Lett. **84** (2000) 4300.

[22] OPAL Collaboration, *“A study of b Quark Fragmentation into* B^0 *and* B^+ *Mesons at LEP”*, Phys. Lett. **B364** (1995) 93.